

# 1    **Translational contributions to tissue-specificity in rhythmic and constitutive gene** 2    **expression**

3    Violeta Castelo-Szekely<sup>1</sup>, Alaaddin Bulak Arpat<sup>1,2</sup>, Peggy Janich<sup>1</sup>, David Gatfield<sup>1,\*</sup>

4    <sup>1</sup> Center for Integrative Genomics, Génopode, University of Lausanne, and <sup>2</sup> Vital-IT, Swiss Institute of  
5    Bioinformatics, 1015 Lausanne, Switzerland

6    \* corresponding author: david.gatfield@unil.ch

7    Tel. +41 21 6923994

8    Fax. +41 21 6923905

9    Running title: Cross-organ analysis of translation

10    Keywords: circadian clocks, translation, ribosome profiling, kidney, liver

## 11 **Abstract**

12 The daily gene expression oscillations that underlie mammalian circadian rhythms show striking tissue  
 13 differences and may involve post-transcriptional regulation. Both aspects remain poorly understood. We  
 14 have explored the contribution of translation efficiency to temporal gene expression by ribosome profiling  
 15 in kidney, and contrasted it with liver data available from the same mice. We observed that rhythmic  
 16 translation of constantly abundant transcripts was markedly organ-specific. Moreover, translation  
 17 efficiency modulated the timing of protein biosynthesis from rhythmic mRNAs and the expression of core  
 18 clock components, consistent with organ-specificity in clock parameters and clock output gene  
 19 repertoires. Our comprehensive datasets provide insights into translational control beyond temporal  
 20 regulation. Transcriptome-wide, cross-organ differences in translation rate were widespread and resulted  
 21 in a phenomenon of translational compensation of constitutive mRNA differences between the tissues.  
 22 The unique resources provided through our study will serve to address fundamental questions of post-  
 23 transcriptional control and differential gene expression *in vivo*.

24 Reviewer link to deposited data:

25 (available on request)

Circadian clocks serve organisms to anticipate daily recurring changes in the environment and to synchronize behaviour, physiology and gene expression according to time of day. The mammalian circadian system consists of a master clock in the brain's suprachiasmatic nuclei (SCN) that receives photic inputs from the retina and synchronizes peripheral clocks present in most cells throughout the body. The molecular timekeeping mechanism – the core clock – relies on a network of transcriptional activators and repressors interacting in negative feedback loops (reviewed in<sup>2,3</sup>). In the core loop, the heterodimeric transcription factor ARNTL:CLOCK (also known as BMAL1:CLOCK) drives the expression of its own repressors, encoded by the *Period* (*Per1*, *Per2*, *Per3*) and *Cryptochrome* (*Cry1*, *Cry2*) genes – a configuration also known as the positive and negative limbs of the oscillator. Additional feedback – in particular an interconnecting limb involving nuclear receptors of the REV-ERB (encoded by genes *Nr1d1*, *Nr1d2*) and ROR (*Rora*, *Rorb*, *Rorc*) family – intersects with the core loop, and numerous post-translational modifications of clock proteins further add to the complexity of the circuitry. The final outcome is a set of robustly cycling transcriptional activities peaking at different phases around the day that drive the rhythmic expression of hundreds to thousands of other genes, termed the clock output or clock-controlled genes (CCGs). It is noteworthy that, despite the probably (near-)identical molecular makeup of the core clock across cell types, CCGs show considerable tissue-specificity<sup>4</sup>. The co-regulation by core clock and tissue-specific (non-rhythmic) transcription factors may engender such cell type-specific rhythmic expression patterns, as shown to occur in *Drosophila*<sup>5</sup>. Overall, however, the origins of tissue-specificity in rhythmic gene output (and even in certain core clock parameters<sup>6</sup>) are poorly understood. Mechanisms that act at the post-transcriptional level and that impact daily mRNA and protein accumulation kinetics are plausible players in the generation of cell type differences as well.

Rhythmic gene expression has been mainly investigated at the transcriptome level i.e., using mRNA abundances as a primary readout. However, comparison of mRNA levels with datasets of genome-wide transcriptional activity and of protein abundances that have become available recently, has suggested that a surprisingly large fraction of gene expression oscillations may have post-transcriptional origins (reviewed in<sup>7</sup>). The many cases of protein rhythms that are independent of an underlying oscillating transcript (initially reported in a low-throughput mass-spectrometric study from mouse liver already 10

years ago<sup>8</sup> and recently confirmed at a comprehensive scale<sup>9,10</sup>) point to important roles for translation, protein degradation and protein secretion in shaping time of day-dependent proteomes. We<sup>1</sup> and others<sup>11</sup> have recently used ribosome profiling, a genome-wide method that assesses translation efficiency through the deep sequencing of ribosome-protected mRNA fragments, to chart the contribution of translational control to daily protein biosynthesis in mouse liver. One conclusion that emerged from the identified cases of translationally generated oscillations was that circadian clock activity and feeding rhythms both contribute to the regulation of rhythmic gene expression output<sup>1,11</sup>. Notably, the most abundant group of transcripts subject to rhythmic translation, i.e. mRNAs encoding ribosomal proteins and other components of the translation machinery that all contain 5'-terminal oligopyrimidine tract (5'-TOP) sequences responsive to the mammalian target of rapamycin (mTOR) regulation<sup>12</sup>, appear to be under the dominant control of feeding<sup>11</sup>.

Analogous to our liver datasets<sup>1</sup>, we have performed ribosome profiling using a second organ from the same cohort of animals, the kidney, which is an emerging circadian model organ with distinct rhythmic functions<sup>13</sup>. By contrasting kidney and liver datasets we comprehensively assessed commonalities and differences in their translomes, and we evaluated in how far the regulation of translation efficiency contributed to tissue specificity in rhythmic and constitutive protein biosynthesis.

## Results

### Around-the-clock ribosome profiling datasets from two organs

For our recent study of the liver translome around-the-clock<sup>1</sup> we had used ribosome profiling<sup>14</sup> (RPF-seq) on a time series of organs collected from mice sacrificed every 2 hours over the 24-hour day (12 timepoints in duplicate; Fig. 1A). To generate a complementary dataset from a second organ we chose the kidneys from the same cohort of animals. Liver and kidney express thousands of genes in common<sup>4,15</sup>, thus providing a particularly suitable setting for a cross-organ comparison of gene expression regulation. Applying the same experimental and computational methods as for liver RPF-seq<sup>1,16</sup>, we obtained comparable high-quality data for kidney (see Supplementary Table S1 and Supplementary Fig. S1A-C for details on sequencing and mapping outcomes). Briefly, ribosome footprints from both organs were



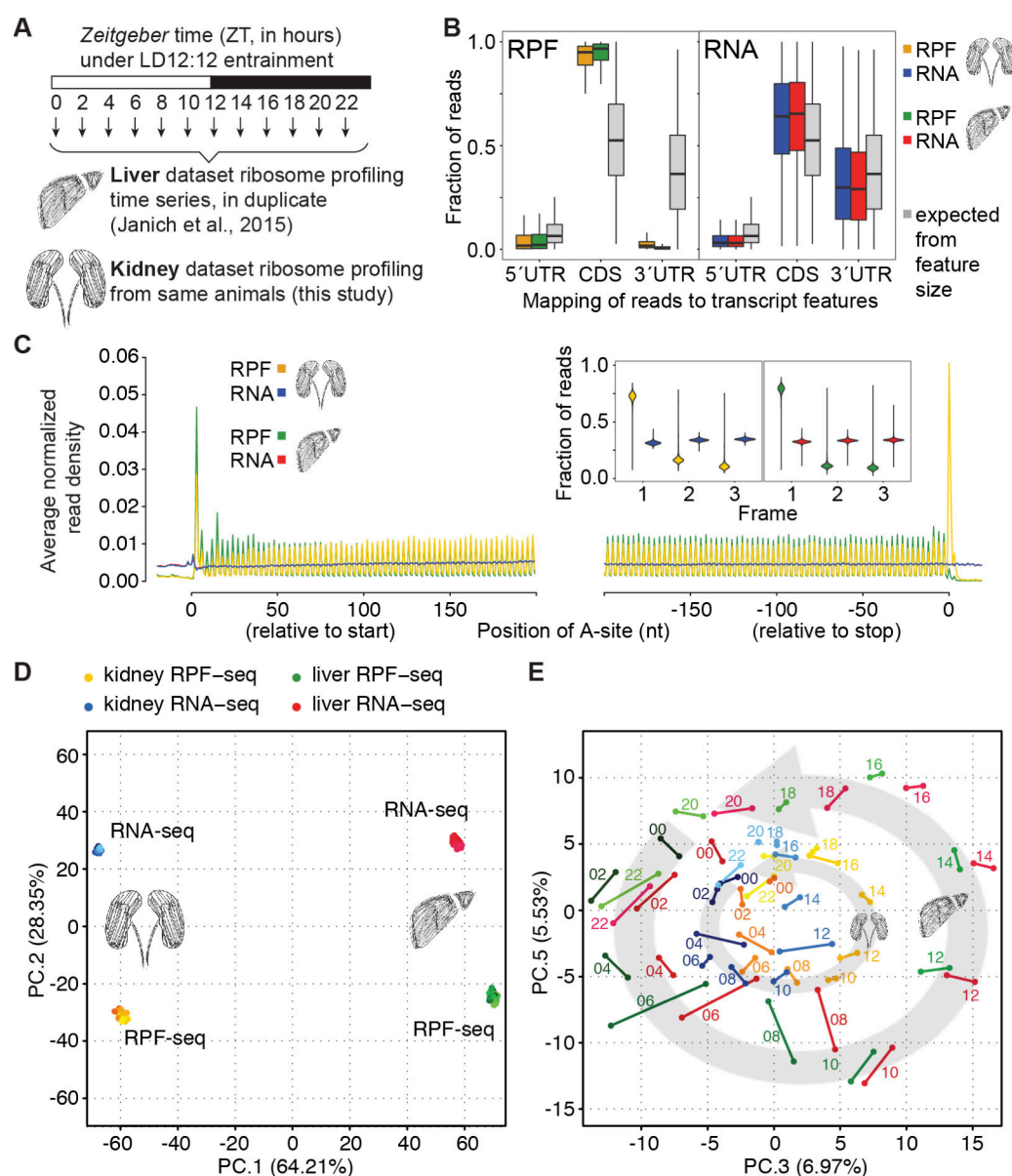


**Figure 1. Ribosome profiling around-the-clock in mouse liver and kidney.**

**(A)** Overview of the experimental design: livers and kidneys from the same mice were collected every 2 hours for two daily cycles and ribosome profiling was performed. Each timepoint sample was a pool of two mice livers or kidneys. Animals were kept under 12 hour:12 hour light-dark conditions, with *Zeitgeber* times ZT00 corresponding to lights-on and ZT12 to lights-off. **(B)** Read distribution within the transcripts' 5' UTRs, CDS and 3' UTRs for RPF-seq (left; yellow and green for kidney and liver, respectively) and RNA-seq (right; blue and red for kidney and liver, respectively) compared to a distribution expected from the relative feature sizes (grey). As the distributions based on the feature sizes were highly similar for both organs, only that for one organ (kidney) is shown. Note that RPF-seq footprints were enriched on the CDS and depleted from UTRs, whereas RNA-seq reads distributed more homogeneously along the transcript, according to feature size. **(C)** Predicted position of the ribosome's aminoacyl tRNA-site (A-site) of reads relative to the CDS start and stop codons. Read density at each position was averaged across single protein isoform genes (i.e. genes with one expressed transcript isoform) that had an average RPF RPKM > 5, a CDS > 400 nt in length and were expressed in both organs (n=3037 genes). This analysis revealed the trinucleotide periodicity of RPF-seq (but not RNA-seq) reads in both organs. *Inset*: Frame analysis of CDS reads showed preference for the annotated reading frame (i.e. frame 1) in RPF but not RNA-seq reads. Violin plots extend to the range of the data (n=3694 genes for liver, n=4602 genes for kidney). **(D)** Principal component (PC) analysis of kidney and liver RPF-seq and RNA-seq datasets, using the top-4000 most variable genes. The first two components reflected the variability coming from organ (64.21%) and from RPF/RNA origin of datasets (28.35%). **(E)** PC3 vs. PC5 (together 12.5% of variation) sequentially resolved the factor time within each dataset, resembling the face of a clock. Each dot represents a timepoint sample, replicates are joined by a line and timepoints within each dataset are sequentially colored. The circular arrangement of the liver data was larger than that of kidney, indicating a higher contribution of hepatic rhythmic genes to overall variability. A scree plot of the ten first PCs and a representation of PC4 can be found in Supplementary Fig. S3.

similarly enriched for protein coding sequences (CDS) of mRNAs and depleted of untranslated regions (UTRs) (Fig. 1B). Like the footprints from liver, also those from kidney exhibited excellent reading frame preference, which allowed resolving the 3-nt periodicity of coding sequences transcriptome-wide (Fig. 1C). Moreover, the high correlation coefficients seen across replicates of the kidney time series for both RNA- and RPF-seq data indicated excellent biological and technical reproducibility (Supplementary Fig. S2A-B). Finally, principal component (PC) analysis on all available datasets (96 libraries, i.e. RPF-seq and RNA-seq from 2 organs, over 12 timepoints, and in duplicate) segregated the data according to the main experimental and biological covariates. PC1 (explaining 64.2% of variation) thus separated libraries according to organ, indicating that tissue origin represented the major source of divergence, followed by PC2 (28.4%) that separated RNA-seq (mRNA abundance) and RPF-seq (footprints/translation) (Fig. 1D). The cyclic nature of the data was resolved in the representation PC3 vs. PC5 (together 12.5%), in which timepoints assembled to a near-perfect clock (Fig. 1E). The larger circular arrangement of the liver vs. kidney time series suggested that rhythmic gene expression in the liver contributed more strongly to overall variation than did kidney rhythms. This observation is in line with the notion that there are more rhythmic transcripts in liver than in kidney and that hepatic oscillations are overall of higher amplitude<sup>4</sup>. Of the further components of the PCA (Supplementary Fig. S3A), PC4 (5.94% of variation) was remarkable as it grouped RNA-seq from one organ with RPF-seq from the other organ (Supplementary Fig. S3B). A plausible interpretation of this observation was the occurrence of translational buffering, which has recently been described in other systems<sup>17,18</sup> and which compensates divergent RNA expression to lead to higher similarity at the level of protein biosynthesis (i.e., ribosome footprints). Taken together, we concluded that the kidney data were of similar high quality as our previous liver datasets<sup>1</sup> and would be suitable for comparative analyses of time of day-dependent and constitutive translation across two tissues.

**Cross-organ differences in translation efficiency are widespread, of moderate scale, and partially compensate RNA abundance differences**

To what extent differences in translation rate contribute to organ-specific gene expression output is still unclear. To address this question we first selected the common transcript set using identical cut-offs on RPKM (reads per kilobase of transcript per million mapped reads) for both organs. We identified 10289 genes whose expression was detectable at both levels, RPF and RNA, in kidney and liver (Fig. 2A). Cross-organ comparison of RPF and RNA data revealed that footprint abundances correlated consistently better between liver and kidney than did transcript abundances (Spearman  $\rho$  [RPF]: mean 0.784 vs.  $\rho$  [RNA]: mean 0.736;  $p=1.19e-07$ ; Wilcoxon signed rank test) (Fig. 2B; Supplementary Fig. S2C-D). This finding lends support to the notion that differences in mRNA expression across tissues are partially compensated by counteracting effects on translation rate, leading to convergence at the level of protein biosynthetic output. Of note, this idea is conceptually similar to suggestions that proteomes are evolutionarily more highly conserved than transcriptomes<sup>19,20</sup>.

From the ratio of CDS-mapping RPF-seq to RNA-seq reads we next calculated relative translation efficiencies (TEs) per transcript and for each organ. We first quantified the degree to which TE differences contributed to organ-specific gene expression output. These analyses revealed that TEs were overall rather similar between organs, as 95% of genes fell into a less than 3-fold range for the kidney/liver relative TE ratio (Fig. 2C). By contrast, this range was greater than 100-fold for the transcript abundance ratio. Given that already within each organ, mRNA abundances showed a considerably broader spread than TEs (several hundredfold vs. barely greater than tenfold, respectively; Supplementary Fig. S4A-B; see also<sup>1,21</sup>), large differences in TEs between organs were not to be expected and would have been surprising. Together with other recent studies (discussed in<sup>22,23</sup>), our findings make earlier suggestions<sup>24</sup> that translation rates could be particularly good predictors of protein abundances seem improbable. They are rather in line with a dominant role for the regulation of mRNA levels (i.e., transcription and mRNA decay) in controlling gene output.

Despite the overall comparatively narrow dynamic range, TE differences between the organs reached statistical significance for a large proportion of the transcriptome. Comparison of the 24 kidney and matching 24 liver samples conferred high statistical power and yielded 5013 genes whose transcripts' TEs were significantly different between tissues (Wilcoxon signed rank test for paired samples;  $FDR < 0.01$ ); we

further implemented a 1.5-fold cut-off on TE ratio in order to select the cases that showed the strongest regulation, resulting in 960 “TE different” genes (Fig. 2D).

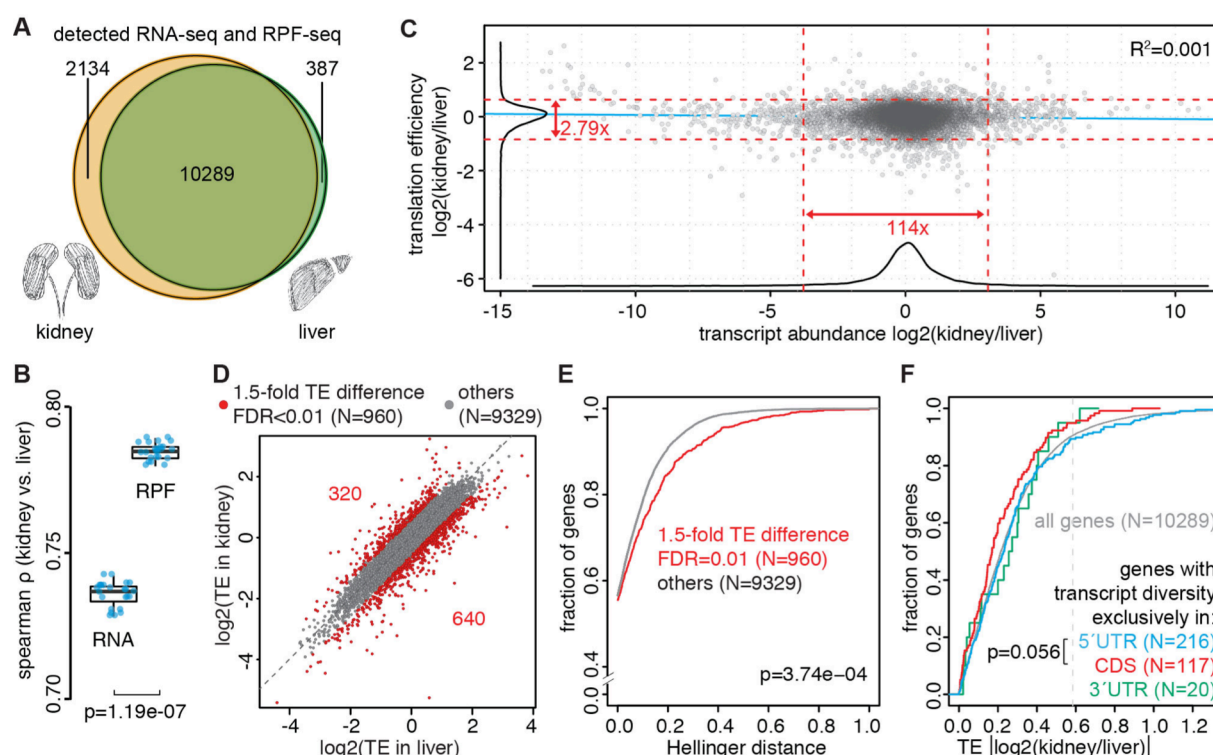


**Figure 2. Widespread cross-organ differences in translation efficiency that are compensatory to RNA abundance differences and show association with transcript features.**

(A) Venn diagram showing the overlap in the expressed genome (i.e. detected at both RPF-seq and RNA-seq levels) between kidney (yellow,  $n=12423$  genes) and liver (green,  $n=10676$  genes). (B) Inter-organ Spearman correlation for RNA-seq and RPF-seq samples. Each dot represents the correlation coefficient for a timepoint and replicate sample. Note that RPF-seq samples consistently correlated significantly better than RNA-seq samples did ( $p=1.19e-07$ ; Wilcoxon signed rank test). (C) Scatterplot of kidney-to-liver ratio of mRNA abundance vs. translation efficiency (TE) for all expressed genes ( $n = 10289$ ), averaged over all timepoints. Corresponding density curves are plotted on the margins. Dashed red lines represent the 2.5 and 97.5 percentiles of each variable, and the corresponding fold-change is indicated. Linear regression line is depicted in blue ( $R^2=0.0009$ ,  $p=0.0009$ ). While 95% of genes spanned a 114-fold range in mRNA abundance differences across organs, the same number of genes changed less than 3-fold in TE, indicating that transcript abundance was the main contributor to divergent gene expression output. (D) Relative TE in liver vs. kidney, centered and averaged over all timepoints for all expressed genes ( $n=10289$ ), showed an overall inter-organ correlation (grey,  $n=9329$ ). However, differential TE was detected for ~9% genes (red,  $n=960$ ). Differential TE genes are defined as having FDR-corrected  $p$ -value  $< 0.01$  (Wilcoxon signed rank test on TE) and  $>1.5$  difference in TE across organs. (E) Cumulative distribution of Hellinger distances for genes showing differential TE (red,  $n=960$ ), or not (grey,  $n=9329$ ), as detected in (D). Hellinger distance was used as a measure to quantify how divergent transcript isoform usage was across organs (see Results and Methods); the analysis shows that divergent TE correlated with larger diversity in transcript isoform expression ( $D=0.0702$ ,  $p=3.74e-04$ , two-sample Kolmogorov-Smirnov [KS] test). (F) Cumulative distribution of the absolute kidney-to-liver TE ratio for genes whose transcript diversity originated only from the 5' UTR (blue,  $N=216$ ), only from the CDS (red,  $N=117$ ) or only from the 3' UTR (green,  $N=20$ ). The vertical dotted grey line marks the 1.5-fold difference used to define differential TE (as in (D)). Although the difference between the “5' UTR diversity only” and the “CDS diversity only” distributions did not reach statistical significance ( $D=0.15349$ ,  $p=0.056$ , two-sample KS-test), these results suggested that tissue specificity in TE was partially achieved by expressing transcript isoforms that differ in their 5' UTR.

We next examined whether any overt transcript characteristic would have predictive value for differential TE. Remarkably, however, we were unable to identify any single, dominant mRNA feature that could potentially indicate an underlying mechanism. For example, we had previously observed that in the liver the presence of a translated upstream open reading frame (uORF) in the 5' UTR had strong predictive value for low TE<sup>1</sup>. An analogous analysis on the kidney datasets revealed a comparable relationship between uORF usage and low TE in this organ as well (Supplementary Fig. 4C). Nevertheless, we were unable to detect a significant correlation between differential uORF usage and TE differences of transcripts across organs (data not shown; see also below, Fig. 5F). Similarly, the 960 "TE different" transcripts were not enriched for any predicted miRNA binding sites, making it unlikely that this class of post-transcriptional regulators is a major player in establishing tissue-specific TEs (data not shown).

The only feature that we identified as significantly associated with differential TE was transcript isoform diversity between the two organs i.e., the occurrence of tissue-specific mRNA variants generated by alternative transcriptional start sites, by alternative splicing, and by alternative 3' cleavage/polyadenylation sites (Fig. 2E). In short, in this analysis we first used the RNA-seq data to compile an inventory of the annotated, protein-coding transcript isoforms and their estimated relative expression levels for each gene and separately for both tissues. We then used the Hellinger distance<sup>25</sup> as a measure of dissimilarity of isoform expression levels between kidney and liver. A value of 0 for this metric signifies that a gene has an identical distribution of isoform expression levels between the tissues and a value of 1 indicates the lack of overlap in expressed isoforms. Globally, "TE different" genes showed significantly higher Hellinger distances than the remainder of the expressed genes ( $p=3.74e-04$ ; Kolmogorov-Smirnov-test) (Fig. 2E). TE differences between tissues may therefore, at least in part, have their origin in tissue-specific transcript variants. However, it is important to note that this mechanism can potentially account only for some of the observed TE divergence, as slightly over half of all expressed genes, including those within the "TE different" set, showed Hellinger distance of 0 (i.e., the same, single protein-coding transcript isoform was expressed in kidney and liver) (Fig. 2E). Molecularly, the term "transcript isoform" comprises variations in mRNA structure that can affect 5' UTR, CDS, 3' UTR, or frequently combinations thereof. To evaluate whether any particular such variation would be more

predictive of TE differences than another, we selected the genes for which the expressed variants affected only one single feature (5' UTR, CDS, or 3' UTR), omitting the more common, but potentially complicated combinatorial cases from our analysis. We found that transcript diversity affecting the 5' UTR was more highly associated with differential TE than was CDS diversity (Fig. 2F). Of note, the association of the 5' UTR with TE is in line with the common view that initiation is rate-limiting for translation and that structure and sequence at and upstream of the translational start determine the efficiency with which scanning ribosomes commit to a productive engagement. Unfortunately, the low number of transcripts that showed exclusive 3' UTR diversity (20 genes) precluded a reasonable interpretation of this feature, and although the generally low number of genes available for all three groups limited the statistical power of our analyses, it is remarkable that the difference between 5' UTR and CDS only marginally failed the commonly used threshold of statistical significance ( $p=0.056$ ; Kolmogorov-Smirnov-test) (Fig. 2F). Finally, we were interested in whether cross-organ differences in TE were associated with functional classes of transcripts. For the 640 "TE different" genes that showed increased translation rate in liver (Fig. 2D), gene ontology (GO) analyses revealed significant enrichment for categories related to transcription (Supplementary Table S2). Conceivably, tissue-specific translational control of transcriptional regulators may thus impact also on the organs' transcriptomes. The 320 "TE different" genes that were translated better in kidney (Fig. 2D) did not show any significant functional enrichment.

### **Translational modulation of phase of oscillation in kidney**

We next turned to the analysis of factor time across the datasets. In order to annotate rhythmic events for kidney we used the same methodology, including a 1.5-fold cut-off on peak-to-trough amplitudes, as previously for the liver time series<sup>1</sup>. A list of the detected RNA and RPF rhythms and genome-wide gene expression plots can be found in Supplementary Table S3 and in Supplementary Dataset S1, respectively. Our analyses yielded 1338 genes whose RNA abundance oscillated and 977 that cycled at the footprint level, corresponding to 10.8% and 7.9% of expressed genes in kidney (Fig. 3A). The overlap of 542 genes corresponded to 41% and 55% of the "transcript rhythmic" and "footprint rhythmic" cases, respectively (Fig. 3A). However, it is important to note that this rather modest concordance between the rhythmic



RNA and RPF gene sets certainly underestimates the true extent of rhythmicity shared between RNA abundance and ribosome footprints, and overestimates the extent of “RNA only” and “translation only” oscillations. The reasons lie in the propensity of rhythmicity detection algorithms to generate false-negatives, and the lack of a canonical method to reliably determine true absence of rhythms (a common problem in the field that is discussed in a recent review<sup>7</sup>). Therefore, and as in our previous study<sup>1</sup>, we implemented more sophisticated methods to identify the true-positive “translation only” cycling transcripts (see later), and the only sector from the Venn diagram that we analysed at this point were the 542 shared rhythmic gene.

Interestingly, the comparison of RNA abundance and footprint rhythmicity parameters across the 542 genes revealed that the timing of the RPF peaks relative to the RNA peaks had a significantly different and broader distribution than the corresponding set from liver ( $p < 1.0 \times 10^{-4}$ ; permutation test) (Fig. 3B). This finding suggested that the phase of protein biosynthesis rhythms undergoes stronger translational modulation in kidney than it does in liver, where RPF peaks are more tightly gated by RNA abundance peaks. Moreover, it was striking that the kidney data showed the tendency for maximal translation to *precede* maximal mRNA abundance (Fig. 3C). Although the mean RPF peak time advance (-0.123 hours) did not reach statistical significance ( $p = 0.16$ , Wilcoxon rank sum test), the large number of transcripts (282) for which the rhythm of translation was phase-advanced to its RNA accumulation was intriguing.

A shortcoming of the above phase analysis is that we compared different rhythmic gene sets in the two organs. The alleged tissue differences in the RPF-RNA phase relationships could therefore have simply arisen from transcript-specific rather than tissue-specific differences in the timing of translation. We therefore determined the common rhythmic transcript set by overlapping kidney and liver with regard to rhythmic events (Fig. 3D). A group of 178 genes (that included most core clock components; Supplementary Fig. S5A; Supplementary Table S4; Supplementary Dataset S2), showed rhythmicity throughout, i.e. in both organs at RNA and RPF level. For this transcript set, the distribution of RPF-RNA intervals was significantly broader in kidney than in liver (Fig. 3E;  $p = 0.007$ , permutation test) with an RPF peak phase advance in kidney (mean -0.143 h) and a phase delay in liver (mean 0.036 h) (Supplementary Fig. S5B-C). We next calculated the gene-wise RPF-RNA phase difference in kidney relative to that in liver.

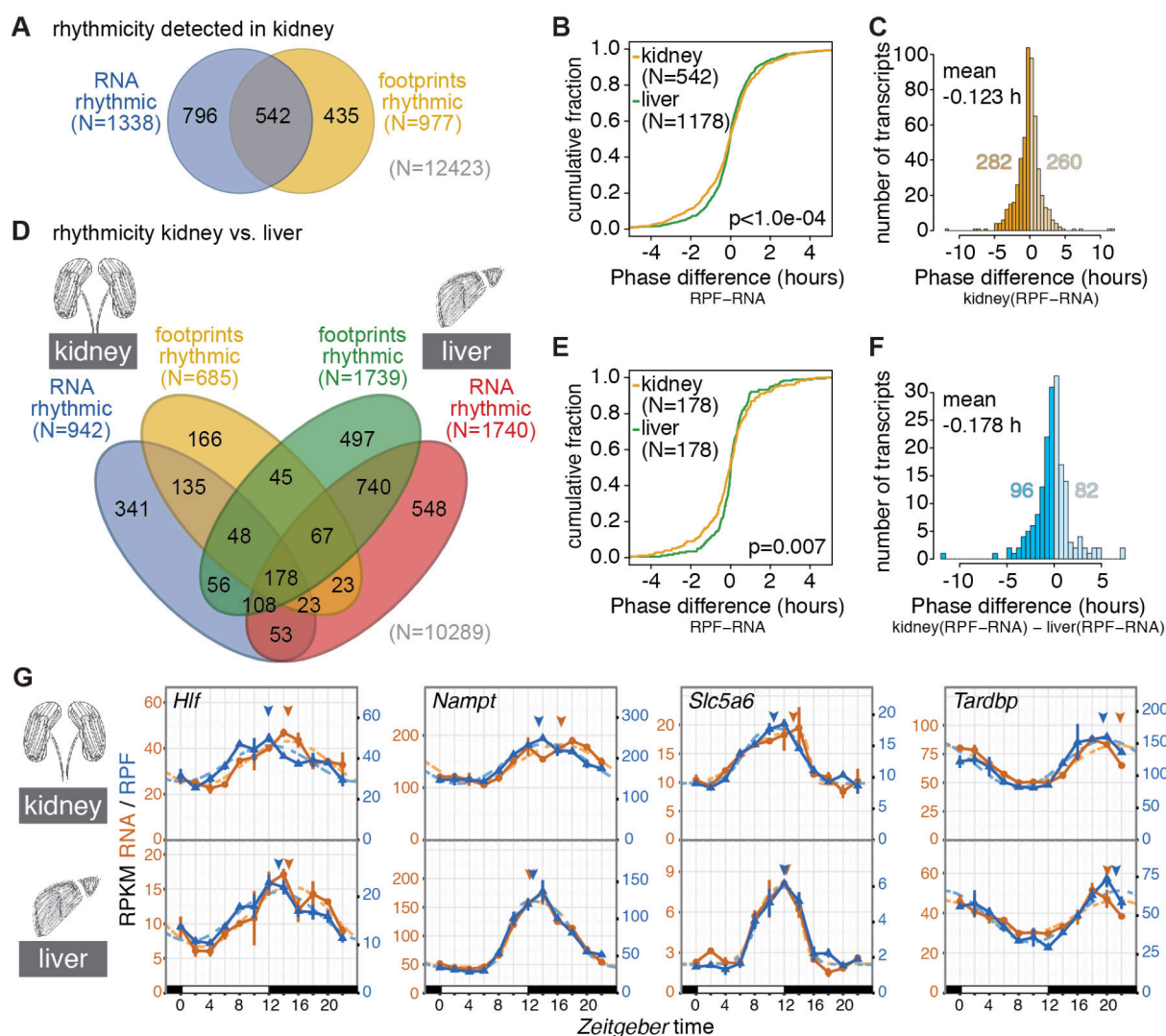


**Figure 3. Rhythmicity analysis across organs and oscillation phase regulation.**

(A) Venn diagram of the rhythmicity analysis in kidney. Of the 12423 genes detected, 1338 showed 24-hour oscillations of >1.5-fold amplitude in mRNA abundance (RNA-seq, 10.7%), 977 in footprints abundance (RPF-seq, 7.9%), and 542 (4.3%) were detected as rhythmic at both levels. 10650 (85.7%) genes were detected as non-rhythmic in our analysis. (B) Cumulative distribution of phase differences (RPF peak - RNA peak, in hours) for genes rhythmic at both RNA-seq and RPF-seq in liver (green, N=1178) and kidney (yellow, N=542). The two distributions were significantly different ( $p < 1e-04$ , permutation test), and reflected that maximal footprint abundance frequently preceded mRNA abundance peaks in kidney (note that the two distributions differed mostly in their negative tail). (C) Histogram of phase differences (RPF-RNA, in hours) for genes rhythmic at both levels in kidney (N=542). Although the distribution mean was not significantly different from 0, more genes had their footprint abundance peaks advanced (N=282) than delayed (N=260) with respect to their mRNA abundance peak. (D) 4-way Venn diagram of rhythmicity sets for genes expressed in both tissues (n=10289). 364 and 238 genes were detected as rhythmic in both organs at the RNA-seq and RPF-seq levels, respectively, and 178 genes were detected as rhythmic throughout (i.e. at RNA-seq and RPF-seq, in kidney and in liver). (E) Cumulative phase difference distribution in liver (green) and kidney (yellow) for the 178 genes rhythmic throughout. As in (B), the distributions were significantly different ( $p=0.007$ , permutation test), and reinstated that even when comparing the same set of genes, footprint peaks frequently preceded mRNA abundance maxima in kidney. (F) Histogram of the differential (kidney - liver) phase delay (RPF - RNA) for the 178 genes rhythmic throughout. (G) Daily profiles of RPF-seq RPKM (blue) and RNA-seq RPKM (orange) for four representative genes in which footprint abundance peaks preceded by several hours maximal mRNA abundance in kidney (top) but not, or less so, in liver (bottom). Arrowheads indicate the peak in footprint and mRNA abundance in their respective colors as estimated by the rhythmic fits.



More genes showed their RPF peaks advanced (96) than delayed (82) in kidney vs. liver, with a mean phase advance that amounted to -0.178 hours (Fig. 3F). Although the phase advance globally did not reach statistical significance ( $p=0.152$ , Wilcoxon rank sum test), visual inspection of the RNA and RPF profiles identified numerous compelling cases of transcripts where specifically in kidney translation peaked up to several hours ahead of maximal RNA abundance, as shown by the examples *Hlf* (Hepatic leukemia factor, a circadian PAR-domain basic leucine zipper transcription factor), *Nampt* (Nicotinamide phosphoribosyltransferase, an enzyme involved in NAD biosynthesis), *Slc5a6* (solute carrier family 5 member 6, a sodium-dependent transporter for biotin and other vitamins) and *Tardbp* (TAR DNA binding protein) (Fig. 3G).

Translation that is phase-advanced to mRNA abundance is counterintuitive at first sight. Conceivably, however, it may occur when the translation rate is not constant over the lifetime of the mRNA but decreases, e.g. as a result of its gradual deadenylation<sup>26</sup>. In keeping with this hypothesis, we have observed that most subunits of the major cytoplasmic deadenylase complex, CCR4-NOT, are significantly more highly expressed in kidney than in liver (Supplementary Fig. S6A-C). Higher deadenylase activity in kidney could provide an attractive molecular explanation for the observed tissue-specific differences in RPF-RNA phasing, and for RPF rhythms that are phase-advanced to RNA rhythms.

### High tissue divergence in translationally driven rhythms

The aforementioned predisposition of rhythmicity detection methods to yield false-negatives, which was confirmed in our liver study<sup>1</sup> and evident in the kidney datasets as well (Supplementary Fig. S7), reinforced the notion that Venn diagrams that simply overlap rhythmic gene sets need to be interpreted with caution. Specifically, it led to an overestimation of the number of “RNA only” and of “footprints only” rhythmic genes (Supplementary Fig. S7B, D). In order to identify the rhythmically translated, constantly abundant transcripts in kidney with higher confidence, we implemented the analytical framework *Babel*<sup>27</sup> that we had previously used for the liver data as well<sup>1</sup>, to preselect the transcripts whose translation efficiency changed significantly over the day (and/or whose TEs deviated significantly from the global transcript population). Rhythmicity analyses that were then performed on this gene



subset yielded 92 cases with the sought after temporal profiles of rhythmic translation on non-rhythmic mRNAs (Fig. 4A). Comparison with the 142 genes of the analogous set from liver revealed that translationally driven oscillations in protein biosynthesis showed near-perfect tissue specificity. Only two genes, *Abcd4* (ATP binding cassette subfamily D member 4) and *Lypla2* (lysophospholipase 2), were shared between the organs and, moreover, visual inspection indicated that they were among the least compelling cases of “translation only rhythms” that our method had identified (Fig. 4B).

Marked tissue-specificity was further apparent for the daily timing of rhythmic translational events. The phase histograms thus showed striking differences in the peak time distribution between the organs (Fig. 4C-D; difference in distributions:  $p=1.66e-04$ ;  $W = 17.403$ ,  $df = 2$ ; Watson-Wheeler test for homogeneity of angles). Of note, the enrichment for translational maxima at the light-dark transition (*Zeitgeber* time, ZT10-16; ZT00 corresponds to lights-on and ZT12 to lights-off) that dominated the distribution in liver (Fig. 4D, F) was virtually absent from kidney (Fig. 4C, E). Instead, kidney showed enrichment for transcripts with maximal translation occurring around ZT4 and ZT16. Visual inspection of individual examples confirmed liver- and kidney-specificity of RPF rhythms. The cases of robust translational oscillations that we<sup>1</sup> and others<sup>11,12</sup> had previously identified in liver were thus absent or severely blunted in kidney; of note, this included mRNAs encoding ribosomal proteins that make up the bulk of genes showing a translational surge at the light-dark transition (e.g. *Rps25*, *Rpl23a*), as well as transcripts encoding the transcription factors *Deaf1* (deformed epidermal autoregulatory factor 1) and *Mxi1* (MAX interactor 1), and mRNAs containing iron-responsive elements in their 5' UTRs (e.g. Ferritin light chain 1, *Ft1l*) (Fig. 4G), all of which we had previously reported as translationally rhythmic in liver<sup>1</sup>. Rhythmic translation exclusive to kidney was not significantly enriched for particular pathways (data not shown), and the temporal profiles were overall of lower amplitude than those seen for liver; *Tma7* (Translational machinery associated 7 homolog), *Ddb2* (Damage-specific DNA binding protein 2), *Actg1* (Actin, gamma, cytoplasmic 1) and *Hoxd3* (Homeobox D3; not expressed in liver) were among the most distinct examples (Fig. 4H). We concluded that temporal changes in TE were relatively rare in kidney and overall strikingly tissue-specific, possibly indicating differential sensitivity of the organs to the systemic signals or other mechanisms that drive such protein biosynthesis rhythms. Specifically for the most prominent group of genes subject to daily TE

regulation in liver i.e., transcripts encoding ribosomal proteins (RPs) and other components of the translation machinery, it has been suggested that feeding-dependent mTOR-signaling underlies their translational upsurge at the light-dark transition via a mechanism that involves the 5'-terminal oligopyrimidine (5'-TOP) motifs that these transcripts carry<sup>11,12</sup>, and our findings thus suggest that kidney is less sensitive to the responsible systemic cues. Moreover, the TE comparison between both tissues revealed that in kidney RPs were translated at a higher level throughout the day (Fig. 4I), indicating that the lack in rhythmicity in this organ resulted from an absence of translational repression during the light phase rather than an absence of activation in the dark phase.

### **Translational tuning of core clock gene expression**

Observations such as the signature of translational compensation (Fig. 2B) or the phase modulation of CCGs (Fig. 3E), led us to conclude that the initial transcriptomal gene expression outputs underwent widespread refinement at the translational level. In particular within the core clock circuitry, such regulation could have important consequences. Conceivably, the rate and timing in the biosynthesis of individual clock proteins could underlie known cell type differences in core clock parameters (such as free-running period *ex vivo*/phase of oscillation *in vivo*<sup>6</sup>), in clock output gene repertoires<sup>4</sup>, in oscillator strength and robustness<sup>28,29</sup>, or in clock gene loss-of-function phenotypes<sup>30</sup>. We therefore aimed to gain quantitative insight into core clock protein biosynthesis in the two organs and at all three levels, RNA abundance, protein biosynthetic output (footprints), and translation efficiency. We first investigated RNA-seq RPKMs and TEs in a non-time-resolved fashion (averages over timepoints) in order to compare the cumulative daily production across all clock proteins. We noted that most core clock components showed a considerable degree of organ-specificity in their expression that was readily appreciable in the TE vs. RNA abundance representation with both organs plotted in a single graph (Fig. 5A-B). In this representation, identical amounts of biosynthesised protein (i.e., identical RPF RPKMs) locate along the descending diagonals on which differences in transcript abundance and TE cancel each other out. Interestingly, the majority of core clock genes (*Npas2*, *Cry1*, *Cry2*, *Per1*, *Per2*, *Per3*, *Nr1d1*, *Rorc*) showed, at least some diagonal vectorial component (Fig. 5B), which indicated compensatory TE changes that

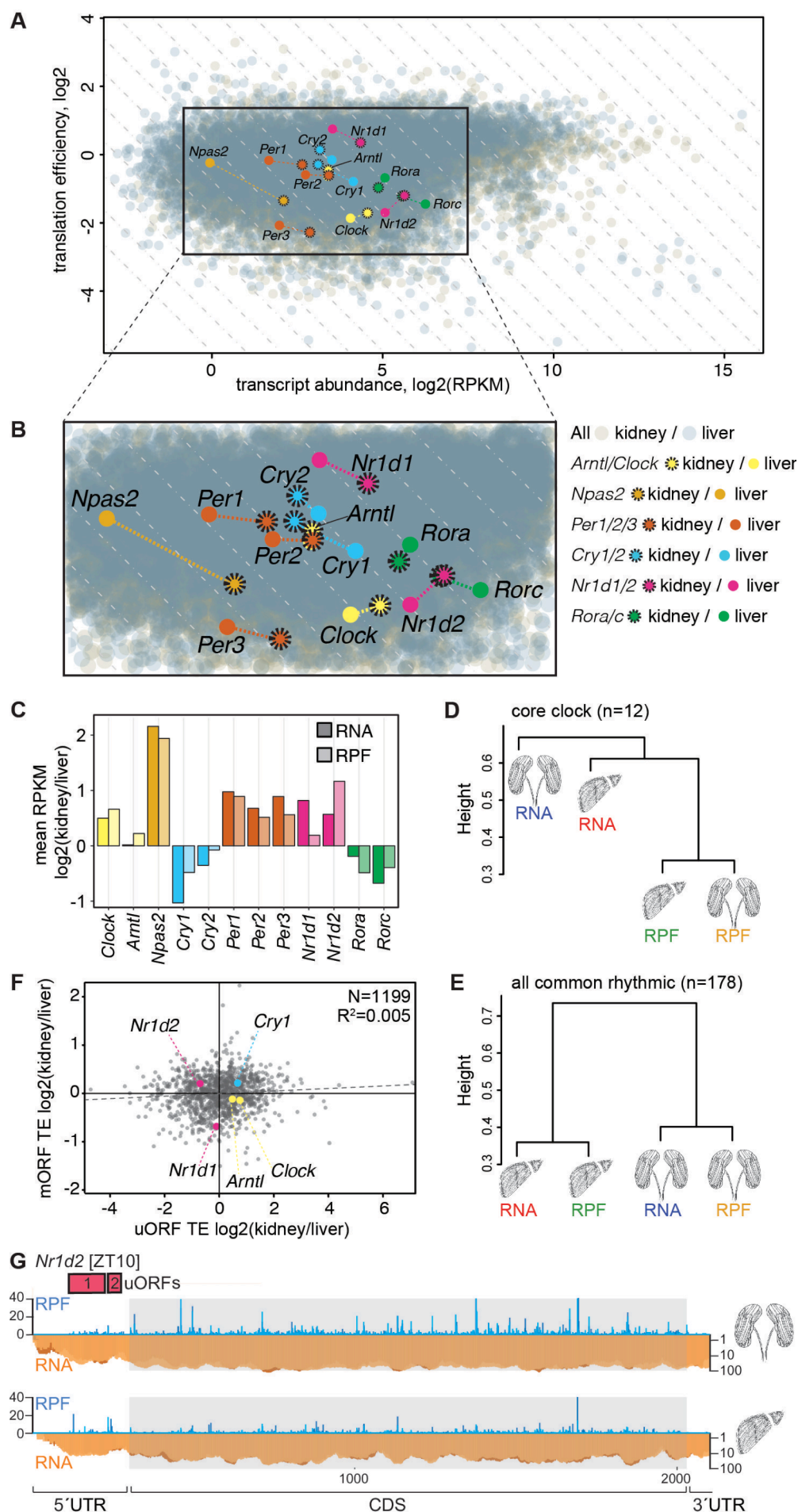




# Figure 5. Translational tuning within the core clock.

**(A)** Scatterplot of transcript abundance vs. translation efficiency for liver (grey) and kidney (sepia), where core clock components are highlighted. Diagonal grey dashed lines indicate same amounts of absolute protein synthesis, where RNA abundance differences are compensated by TE differences. Colored dashed lines join the relative locations of each core clock genes between organs (kidney dots with dashed circles). Note that several core clock components (e.g. *Per* genes, *Cry1*, *Nr1d1*, *Rorc*, *Npas2*) are located along the descending diagonals, suggesting that translational buffering occurs for clock components and counteracts mRNA expression variations. **(B)** Magnification of the indicated area of (A). **(C)** Bar graph of the average RPKM ratio between kidney and liver for the main circadian core clock genes, at the level of mRNA abundance (dark shades) and ribosome footprints (light shades) showed that translational buffering led to a higher similarity at the level of protein biosynthesis (RPF) for several core clock genes. **(D)** Hierarchical clustering of the organs' transcriptomes and translomes based on the similarities of the core clock genes expression patterns (n=12 genes shown in A-C). The height of the branches represents weighted average distances over the considered genes (see Methods). **(E)** Hierarchical clustering of the organs' transcriptomes and translomes based on the similarities in expression patterns of genes detected as rhythmic throughout (i.e. at both RNA and RPF levels in both organs, N=178, see Fig. 3D). The height of the branches represents weighted average distances over the considered genes (see Methods). When compared to the clustering based on core clock gene expression patterns in (D) – for which the higher conservation of protein synthesis levels than mRNA levels was evident – this rhythmic gene set showed an organ-based clustering. **(F)** Scatterplot of upstream ORF (uORF) translation efficiency (TE) vs. main ORF (mORF) TE across organs for genes containing AUG-initiated translated uORFs in both organs (n=1199). uORF-containing core clock genes are highlighted. This analysis showed that differential uORF usage could not globally explain differences in mORF TE across organs (note the lack of negative correlation between the two variables,  $R^2 = 0.005$ ,  $p=0.008$ ). As an exception, the lower uORF TE of *Nr1d2* in kidney might explain its relatively higher mORF TE. **(G)** Raw read distribution for RPF (in blue) and RNA (in orange) along the 5' UTR and CDS of *Nr1d2* in kidney (top) and liver (bottom) for the timepoint of maximal CDS translation. Red boxes indicate AUG-initiated uORFs as predicted in our analyses.

partially counteracted RNA abundance differences between the organs. For *Clock*, *Arntl*, *Nr1d2* and *Rora*, changes in TE exacerbated transcript abundance differences (Fig. 5B-C). The inspection of quantitative relationships between clock components revealed that the main positive (*Clock*, *Arntl*) and negative (*Per1/2*, *Cry1/2*) limb members were all produced in roughly comparable amounts in kidney (i.e., they aligned along a relatively narrow diagonal zone in Fig. 5B), whereas interconnecting limb protein biosynthesis (*Nr1d1/2*, *Rora/c*) was 2-4-fold higher (i.e., they were shifted to the right in Fig. 5B). Overall, we had previously observed a similar pattern in the liver data<sup>1</sup>. Despite such similarity between kidney and liver, however, we also noted two striking manifestations of organ specificity in the amounts and relative ratios of clock protein biosynthesis. First, the interconnecting limb appeared to be subject to “reprogramming”, with an increased biosynthesis of repressive (*Nr1d1/2*) and a decreased production of activating (*Rora/c*) elements in the kidney (Fig. 5C). Of note, beyond functioning in the rhythm-generating clock circuitry, interconnecting limb transcription factors also control an output branch of the oscillator. Consistent with the gene expression differences that we observed (i.e., more activators and less repressors in liver), major loss-of-function phenotypes of interconnecting limb components that have been reported are indeed associated with hepatic pathways, for example with lipid, cholesterol and bile

acid metabolism (e.g.<sup>31,32</sup>). We deem it an attractive hypothesis that by controlling the relative levels of NR1D1/2 vs. RORs, clock output gene repertoires would be tailored in a tissue-specific fashion. Translational mechanisms are likely involved in the regulation, in particular to enhance NR1D2 production in kidney. Second, we observed that within the negative limb, the ratio between PER and CRY biosynthesis was shifted towards increased PERs in kidney (Fig. 5C). PERs (and in particular PER2) are considered stoichiometrically rate-limiting components of the inhibitory complex, and increased PER2 dose engenders long period<sup>33,34</sup>. Consistent with our finding of increased PER production, the kidney clock free-runs with almost 1.5 hour longer period than the liver clock<sup>6</sup>. Conceivably, the modulation of the relative levels of core clock protein production could engender different stoichiometry of the circuitry components and lead to distinct oscillatory parameters of clocks across tissues. Of note, the increase in PER and decrease in CRY biosynthesis in kidney is already established at the transcriptomal level, with TE differences rather leading to partial compensation (Fig. 5B-C).

We next extended the core clock analysis to the time-resolved data. In the expression plots (Supplementary Fig. S8) we calculated for each gene individually the Euclidean distances between the four rhythmic traces (i.e., RNA, RPF in kidney, liver), which served as a measure of similarity between the temporal profiles. Hierarchical clustering of the similarities for the ensemble of the 12 core clock genes showed that RPF rhythms of the two organs grouped together (Fig. 5D), indicating higher similarity of clock protein biosynthesis rhythms between organs than of RNA and RPF rhythms within organs. As a control set, we analysed the 178 common rhythmic genes identified in Fig. 3D, which revealed within-organ clustering (Fig. 5E). These findings underscored that translational compensation was operative within the core clock, leading to more similar rhythms in clock protein biosynthesis than would have been predicted from the rhythmic RNA abundance profiles.

In our previous liver RPF-seq study we had identified uORF translation as a mechanism that is able to regulate the gene expression output for clock components, and we had annotated AUG-initiated uORFs in *Nr1d1*, *Nr1d2*, *Cry1*, *Clock* and *Arntl*<sup>1</sup>. We therefore wished to evaluate whether differential uORF usage could potentially underlie any of the observed cross-organ TE differences for the core clock components. To this end, we calculated the translation efficiency specifically on uORFs (from the ratio of uORF-mapping

RPF to RNA reads; see Methods) for all uORF-containing genes in the two organs, and then correlated uORF TE ratio (kidney/liver) with main ORF TE ratio (kidney/liver) (Fig. 5F). Importantly, given that uORF translation has been associated with decreased initiation at the main ORF<sup>1,35</sup> (see also Supplementary Fig. S4C), we would have expected uORF and main ORF TE ratios to negatively correlate if differential uORF usage were one of the main mechanisms to establish organ-specific TEs. This was, however, globally not the case, and we rather observed weak positive correlation (Spearman  $\rho=0.095$ ). Among individual core clock genes, *Nr1d2* represented the clearest case for negative correlation, showing lower uORF TE and higher main ORF TE in kidney (Fig. 5F). Moreover, negative correlation of uORF- and CDS-mapping footprints in the two organs could be confirmed by visual inspection of raw RPF reads mapping to the *Nr1d2* transcript (Fig. 5G). For *Nr1d2*, differential uORF usage could thus represent a plausible mechanism that contributes to organ-specific protein production, keeping its biosynthesis low in liver and high in kidney.

## Discussion

Along the way from transcription to protein degradation, gene expression can be regulated at numerous levels. Certain steps and intermediates have been particularly well explored, including by genome-wide and quantitative approaches. This has resulted overall in the view that gene expression differences are typically generated transcriptionally and can be conveniently studied at the transcriptomal level. Obviously, however, the functionally relevant output of most gene expression is the protein rather than the transcript. Quantitative, genome-wide analyses of protein biosynthesis are thus of high interest to complement the wealth of available transcriptomics data. Such studies are still scarce because it is only with the recent development of the ribosome profiling technique that a dedicated analysis of translational events in a high-throughput fashion has become possible<sup>14</sup>. Here, we report on a combined analysis of two paradigms of differential gene expression, namely its tissue dependence and its time of day-dependence, to evaluate the contribution of translation to the regulation of gene expression output. We have addressed several, rather fundamental, but still unanswered questions that are of interest to both chronobiology and the gene expression field at large: How does the dynamic range of translation



efficiency compare to that of transcript abundance across two distinct organs? Is translation efficiency a default transcript property and comparable across two tissues, or do TEs become reinterpreted in different cellular environments? Does cross-tissue variability of TEs come with a direction i.e., is there a global tendency to either reinforce or to buffer transcriptomal differences? What is the extent and what are the properties of daily rhythms in translation efficiency, in an organ and between organs? Could differential TE underlie any of the known cross-tissue differences of the clock?

To our knowledge, only one previous study has reported on RPF-seq datasets from two complementary mammalian tissues<sup>18</sup>. The authors recorded datasets from rat liver and heart but, of note, they also included animals with different genetic backgrounds as covariates in the experimental design. The study thus mainly focused on exploring strain differences in translational levels, while tissue differences were not investigated in greater detail. Our choice of liver and kidney (with more than 10'000 commonly expressed transcripts) from the same animals, and the high resolution of the time series, provided high statistical power to our analyses.

Over the last years there has been some dispute regarding the contribution that differences in TE make to gene expression output (recently discussed<sup>22,23</sup>) – including suggestions that TE may actually represent the best predictor of protein abundances<sup>24</sup>. Our data contribute to clarifying some of the disagreement and show that – across genes in a tissue and for individual genes between tissues – the dynamic range of transcript abundances is about 30-50-fold broader than that of translation efficiencies. Gene expression differences are thus mainly set up by differences in transcription (and, possibly, RNA stability), whereas differences in translation rate have more of a modulatory role. It is noteworthy that this modulation is globally characterised by directionality – overall, TE differences thus help to buffer against mRNA abundance differences. Examples for such translational buffering of divergent gene expression (a phenomenon that was also covered in a recent review<sup>23</sup>) have been reported across yeast species<sup>17</sup> and also in the abovementioned study on different strains of rats<sup>18</sup>, and our work extends this concept across organs. As an underlying principle, all these cases of buffering may reflect the fact that selective pressure on precise gene expression levels likely acts on protein abundances and that more tolerance may exist

towards divergence in RNA levels. It will be exciting to study the underpinnings of translational compensation further, across tissues and across species.

At first site, it may appear unsatisfactory that our analyses did not identify specific, dominant transcript features and mechanisms that would explain TE differences between organs. Transcript isoform diversity (in particular at the 5' UTR) may play a role, but for more than half of the transcripts with differential TE, the same, single protein-coding isoform was expressed in both tissues under investigation. Tissue differences in the translation machinery and its regulators – including signalling pathways, the activity of trans-acting factors such as RNA binding proteins (RBPs), translation factors, and even ribosomal composition or tRNA repertoires – are likely involved. They may act in a combinatorial fashion and we expect that a complex translational regulatory universe thus awaits discovery. While ribosome profiling now has allowed us to record the consequences of such regulation at high resolution, understanding all its causes will represent an exciting challenge for the future.

Our study has given rise to novel insights into rhythmic gene expression. The extent to which rhythmicity is generated by the temporal regulation of translation efficiency has been the subject of speculation ever since the first report that many rhythmic proteins in liver are encoded by non-rhythmic mRNAs<sup>8</sup>. Our new kidney datasets complement recent time-resolved ribosome profiling studies from liver<sup>1,11</sup> and from a circadian cell line, U2OS cells<sup>36</sup>. Our comparisons reveal that the number of transcripts subject to translational rhythms is slightly lower in kidney, but overall in a similar order of magnitude as in liver, affecting around 1% of the transcriptome. We were surprised to see that translational rhythms were essentially tissue-specific in terms of the identity of rhythmic translation events and in their phase distribution. A possible explanation is that these rhythms are not driven by local clocks, but by rhythmic systemic cues to which different tissues are not equally responsive. The effects of feeding and mTOR signalling, for example, may be more pronounced in liver than in kidney due to the dedicated role that this organ plays in energy homeostasis and fasting responses. Nevertheless, the lack of rhythmicity of components of the translational machinery (ribosomal proteins) in kidney came as a surprise in the light of previous suggestions of conservation across tissues<sup>12</sup>. In addition to the generation of rhythms by translation (which affected only a relatively small population of transcripts), our analyses have pointed to

a rhythmicity-modulating role affecting the timing of protein biosynthesis oscillations relative to phase of mRNA abundance rhythms. Consistent with work by the Green lab that showed interactions between polyadenylation status of mRNAs and rhythmic protein expression in the liver<sup>26</sup>, it is tempting to speculate that such mechanisms are also operative across organs, with tissue-specific deadenylation kinetics tuning the timing of rhythmic protein biosynthesis.

Historically, the core clock mechanism has been referred to as a “transcription-translation feedback loop” (TTFL; see<sup>37</sup> for an early mention of this term). The actual feedback, however, occurs at the transcriptional level, and possible mechanistic functions of translational regulation have not been much investigated. Our cross-organ comparison of core clock protein biosynthesis suggests that translational control – including through the activity of uORFs<sup>1,36</sup> – is of regulatory interest and represents a way by which the identical set of core clock genes could form circuitries with different stoichiometry of its main components. As a result, both clock parameters and output gene repertoires may be organ-specifically tuned.

## Methods

### Animals

12-week old male mice (C57BL/6J; Janvier Labs) were entrained for two weeks to light:dark 12:12 cycles with *ad libitum* access to food and water and were anesthetized (isoflurane) and sacrificed every two hours (ZT0 - ZT22, with ZT0 corresponding to “lights-on”) for two daily cycles. Livers and kidneys were removed and processed either directly or flash-frozen in liquid N<sub>2</sub>. All experimental procedures were approved by the Veterinary Office of the Canton Vaud (authorisation VD2376).

### Ribosome profiling

Generation of ribosome profiling (RPF-seq) and RNA-seq libraries was described recently<sup>1,16</sup>. Kidney libraries were prepared in the same manner, with one modification. After RNA digestion and recovery of ribosome-protected fragments, 5µg of RNA were treated with Ribo-Zero magnetic kit (Epicentre) according to the manufacturer’s protocol. Ribosomal RNA-depleted samples were then separated in a 15% PAGE gel. Gel was cut to obtain 26-35 nucleotides long fragments and library preparation was continued as done for liver samples and according to the ARTseq ribosome profiling kit instructions (Epicentre). These two steps (Ribo-Zero treatment and PAGE separation) had been inverted during the preparation of our liver samples in order to obtain sufficiently concentrated libraries for sequencing. However, applying this strategy for kidney samples recovered (and sequenced) the rRNA probes of the Ribo-Zero kit intended for rRNA removal from the sample. We reasoned that this might be due to overall lower levels of translation (and therefore relatively less mRNA footprints) in kidney and thus revert the steps back to the original order described by Illumina. RPF and RNA libraries were sequenced on an Illumina HiSeq 2500.

### Sequencing data processing, alignment and quantification

Processing, quality assessment, alignment and quantification of sequencing data were performed as described in our previous study<sup>1,16</sup>. Briefly, sequenced reads were trimmed of their adaptors using Cutadapt<sup>38</sup> and the length distribution of trimmed reads was used to assess the quality of nuclease digestion and size-selection steps, particularly important for RPF libraries (Supplementary Fig. S1B). Next trimmed reads were filtered by size (21-35 for RPF; 21-60 for RNA) using an in-house Python script, and

sequentially mapped to mouse rRNA, human rRNA, mt-tRNA, mouse tRNA, mouse cDNA (Ensemble mouse database release 75) using Bowtie v2.2.1<sup>39</sup> and mouse genome (GRCm38.p2) using Tophat v2.0.11<sup>40</sup>. Trimmed and filtered sequences were also directly mapped against the mouse genome (Tophat) in order to estimate expressed transcript models in each organ (Cufflinks v2.2.1<sup>41</sup>). Transcriptome-mapping reads in the sequential alignment were counted towards their location into the 5' UTR, CDS or 3' UTR of the transcript, based on feature annotation (Ensemble mouse release 75). Mappable and countable feature lengths were not calculated for this study (see "faux reads analysis" in the "Quantification of mRNA and ribosome footprint abundance" section of Supplemental Experimental Procedures of previous study<sup>1</sup>) as its contribution was negligible for further analyses. Therefore no correction factor was applied to RPKM calculations in this study. Read counts in RNA-seq and RPF-seq datasets were normalised with upper quantile method of edgeR<sup>42</sup> and RPKM values were calculated as the number of reads per 1000 bases per geometric mean of normalised read counts per million. Relative translation efficiencies (TE) were calculated as the ratio of RPF-RPKM to RNA-RPKM per gene per sample. Reading frame and nucleotide periodicity analyses were performed as described<sup>1</sup>. Principal Component Analysis (PCA) relied on a combined matrix of CDS counts for RPF and RNA from both liver and kidney, following the same approach as before<sup>1</sup>.

#### **Correlation of RNA-seq and RPF-seq across organs**

Inter-organ correlation at the levels of RNA and RPF-seq (Fig. 2B) was done per timepoint and replicate. Significance of the difference in the spearman coefficient between both distributions was assessed by Wilcoxon rank sum test in R (stats package).

#### **Analysis of differential translation efficiency**

Significance of differences in translation efficiency (TE) between liver and kidney was assessed using the Wilcoxon-rank sum test in R (stats package). A two-sided, paired test was performed on centered TE values per timepoint and replicate, and resulted p-values were FDR-corrected. A gene was defined as having differential TE when FDR < 0.01 and the inter-organ difference in TE was at least 1.5-fold (Fig. 2D).

#### **Analysis of transcript usage diversity across organs**

For each gene  $g$ ,  $P(g) = (p_1, \dots, p_n)$  is the vector of the relative expression proportions of its  $n$  protein-coding transcripts, as estimated in our RNA-seq analysis (see Sequencing data processing, alignment and quantification). To quantify the dissimilarity in relative transcript isoform expression between liver  $L$  and kidney  $K$ , the Hellinger distance  $H^{25}$  is defined as:

$$H(P_L(g), P_K(g)) = 1/\sqrt{2} \sqrt{\sum_{i=1}^n (\sqrt{p_{Li}} - \sqrt{p_{Ki}})^2} \quad (1)$$

Similarity between the distribution of the genes detected as differentially translated (Fig. 2D) and the overall distribution was tested by two-sided two-sample Kolmogorov-Smirnov (KS) test. In order to detect the transcript feature that mostly determines the tissue specificity in translation efficiency, we selected genes whose transcript diversity in both organs originated only from either the 5' UTR, the CDS, or the 3' UTR of the transcripts, based on the annotation information for the protein-coding transcripts detected. Similarity of the "5' UTR-only diversity" distribution to the "CDS-only diversity" distribution was tested with the two-sided two-sample Kolmogorov-Smirnov (KS) test, although the low and very different number of genes in each group ( $n=216$  vs.  $n=117$ ) might limit the power of the test to detect a significant difference between the distributions.

## Rhythmicity analyses

Rhythmicity detection and rhythmic parameters estimation in each dataset (RNA-seq and RPF-seq, liver and kidney) were done based on Akaike information criterion (AIC) model selection as in our previous study<sup>1</sup>. The Babel computational framework<sup>27</sup> was used to detect rhythmically translated genes from constantly expressed mRNAs within each organ.

## Hierarchical clustering of rhythmic genes

In order to study the similarity of rhythmic genes based on their expression profiles, a dissimilarity matrix was computed for each gene of interest, based on the Euclidean distance between the RNA-seq and RPF-seq expression profiles within and across organs. A hierarchical clustering tree was constructed on the weighted average of the dissimilarities matrices under consideration (core clock genes in Fig. 5D or all rhythmic genes in Fig. 5E), using the "average" clustering method. The R functions {packages} dist{stats},

fuse{analogue} and hclust{stats} were used for computing the individual dissimilarity matrices, the weighted mean dissimilarity matrix, and the hierarchical clustering, respectively.

### Upstream open reading frame (uORF) translation efficiency calculation

In order to assess the impact of differential upstream ORFs (uORFs) usage on translation efficiency differences across organs, uORFs were identified as in our previous study<sup>1</sup>. Briefly, genes expressing a single protein-coding isoform in both organs were selected (n=5815) and uORFs starting with an AUG and being at least 18 nucleotides long were considered as translated if they showed significant frame bias towards the first reading frame (relative to the uORF 5') and had a coverage >10%. uORF translation efficiency was calculated from the ratio of RPF-seq to RNA-seq reads on the uORF regions. If several uORFs partially or completely overlapped on a given transcript 5' UTR, a non-overlapping composite uORF was considered for read counting.

### Data access

The sequencing data from this study have been submitted to the NCBI Gene Expression Omnibus (GEO; <http://www.ncbi.nlm.nih.gov/geo/>) under accession number (available on request).

### References

1. Janich, P., Arpat, A. B., Castelo-Szekely, V., Lopes, M. & Gatfield, D. Ribosome profiling reveals the rhythmic liver transcriptome and circadian clock regulation by upstream open reading frames. *Genome research* **25**, 1848-1859, doi:10.1101/gr.195404.115 (2015).
2. Dibner, C., Schibler, U. & Albrecht, U. The mammalian circadian timing system: organization and coordination of central and peripheral clocks. *Annual review of physiology* **72**, 517-549, doi:10.1146/annurev-physiol-021909-135821 (2010).
3. Partch, C. L., Green, C. B. & Takahashi, J. S. Molecular architecture of the mammalian circadian clock. *Trends in cell biology* **24**, 90-99, doi:10.1016/j.tcb.2013.07.002 (2014).
4. Zhang, R., Lahens, N. F., Ballance, H. I., Hughes, M. E. & Hogenesch, J. B. A circadian gene expression atlas in mammals: Implications for biology and medicine. *Proceedings of the National Academy of Sciences of the United States of America* **111**, 16219-16224, doi:10.1073/pnas.1408886111 (2014).

5. Meireles-Filho, A. C., Bardet, A. F., Yanez-Cuna, J. O., Stampfel, G. & Stark, A. cis-Regulatory Requirements for Tissue-Specific Programs of the Circadian Clock. *Current biology : CB* **24**, 1-10, doi:10.1016/j.cub.2013.11.017 (2014).
6. Yoo, S. H. *et al.* PERIOD2::LUCIFERASE real-time reporting of circadian dynamics reveals persistent circadian oscillations in mouse peripheral tissues. *Proceedings of the National Academy of Sciences of the United States of America* **101**, 5339-5346, doi:10.1073/pnas.0308709101 (2004).
7. Luck, S. & Westermark, P. O. Circadian mRNA expression: insights from modeling and transcriptomics. *Cellular and molecular life sciences : CMLS* **73**, 497-521, doi:10.1007/s00018-015-2072-2 (2016).
8. Reddy, A. B. *et al.* Circadian orchestration of the hepatic proteome. *Current biology : CB* **16**, 1107-1115, doi:10.1016/j.cub.2006.04.026 (2006).
9. Mauvoisin, D. *et al.* Circadian clock-dependent and -independent rhythmic proteomes implement distinct diurnal functions in mouse liver. *Proceedings of the National Academy of Sciences of the United States of America* **111**, 167-172, doi:10.1073/pnas.1314066111 (2014).
10. Robles, M. S., Cox, J. & Mann, M. In-vivo quantitative proteomics reveals a key contribution of post-transcriptional mechanisms to the circadian regulation of liver metabolism. *PLoS genetics* **10**, e1004047, doi:10.1371/journal.pgen.1004047 (2014).
11. Atger, F. *et al.* Circadian and feeding rhythms differentially affect rhythmic mRNA transcription and translation in mouse liver. *Proceedings of the National Academy of Sciences of the United States of America* **112**, E6579-6588, doi:10.1073/pnas.1515308112 (2015).
12. Jouffe, C. *et al.* The circadian clock coordinates ribosome biogenesis. *PLoS biology* **11**, e1001455, doi:10.1371/journal.pbio.1001455 (2013).
13. Bonny, O., Vinciguerra, M., Gumz, M. L. & Mazzocchi, G. Molecular bases of circadian rhythmicity in renal physiology and pathology. *Nephrology, dialysis, transplantation : official publication of the European Dialysis and Transplant Association - European Renal Association* **28**, 2421-2431, doi:10.1093/ndt/gft319 (2013).
14. Ingolia, N. T. Ribosome profiling: new views of translation, from single codons to genome scale. *Nature reviews. Genetics* **15**, 205-213, doi:10.1038/nrg3645 (2014).



15. Brawand, D. *et al.* The evolution of gene expression levels in mammalian organs. *Nature* **478**, 343-348, doi:10.1038/nature10532 (2011).
16. Janich, P., Arpat, A. B., Castelo-Szekely, V. & Gatfield, D. Analyzing the temporal regulation of translation efficiency in mouse liver. *Genomics data* **8**, 41-44, doi:10.1016/j.gdata.2016.03.004 (2016).
17. McManus, C. J., May, G. E., Spealman, P. & Shteyman, A. Ribosome profiling reveals post-transcriptional buffering of divergent gene expression in yeast. *Genome research* **24**, 422-430, doi:10.1101/gr.164996.113 (2014).
18. Schafer, S. *et al.* Translational regulation shapes the molecular landscape of complex disease phenotypes. *Nature communications* **6**, 7200, doi:10.1038/ncomms8200 (2015).
19. Khan, Z. *et al.* Primate transcript and protein expression levels evolve under compensatory selection pressures. *Science* **342**, 1100-1104, doi:10.1126/science.1242379 (2013).
20. Schrimpf, S. P. *et al.* Comparative functional analysis of the *Caenorhabditis elegans* and *Drosophila melanogaster* proteomes. *PLoS biology* **7**, e48, doi:10.1371/journal.pbio.1000048 (2009).
21. Ingolia, N. T., Lareau, L. F. & Weissman, J. S. Ribosome profiling of mouse embryonic stem cells reveals the complexity and dynamics of mammalian proteomes. *Cell* **147**, 789-802, doi:10.1016/j.cell.2011.10.002 (2011).
22. Li, J. J. & Biggin, M. D. Gene expression. Statistics requantitates the central dogma. *Science* **347**, 1066-1067, doi:10.1126/science.aaa8332 (2015).
23. Liu, Y., Beyer, A. & Aebersold, R. On the Dependency of Cellular Protein Levels on mRNA Abundance. *Cell* **165**, 535-550, doi:10.1016/j.cell.2016.03.014 (2016).
24. Schwanhauser, B. *et al.* Global quantification of mammalian gene expression control. *Nature* **473**, 337-342, doi:10.1038/nature10098 (2011).
25. Gonzalez-Porta, M., Calvo, M., Sammeth, M. & Guigo, R. Estimation of alternative splicing variability in human populations. *Genome research* **22**, 528-538, doi:10.1101/gr.121947.111 (2012).

26. Kojima, S., Sher-Chen, E. L. & Green, C. B. Circadian control of mRNA polyadenylation dynamics regulates rhythmic protein expression. *Genes & development* **26**, 2724-2736, doi:10.1101/gad.208306.112 (2012).
27. Olshen, A. B. *et al.* Assessing gene-level translational control from ribosome profiling. *Bioinformatics* **29**, 2995-3002, doi:10.1093/bioinformatics/btt533 (2013).
28. Lee, Y., Chen, R., Lee, H. M. & Lee, C. Stoichiometric relationship among clock proteins determines robustness of circadian rhythms. *The Journal of biological chemistry* **286**, 7033-7042, doi:10.1074/jbc.M110.207217 (2011).
29. Yagita, K. *et al.* Development of the circadian oscillator during differentiation of mouse embryonic stem cells in vitro. *Proceedings of the National Academy of Sciences of the United States of America* **107**, 3846-3851, doi:10.1073/pnas.0913256107 (2010).
30. Landgraf, D., Wang, L. L., Diemer, T. & Welsh, D. K. NPAS2 Compensates for Loss of CLOCK in Peripheral Circadian Oscillators. *PLoS genetics* **12**, e1005882, doi:10.1371/journal.pgen.1005882 (2016).
31. Le Martelot, G. *et al.* REV-ERB $\alpha$  participates in circadian SREBP signaling and bile acid homeostasis. *PLoS biology* **7**, e1000181, doi:10.1371/journal.pbio.1000181 (2009).
32. Raspe, E. *et al.* Identification of Rev-erb $\alpha$  as a physiological repressor of apoC-III gene transcription. *J Lipid Res* **43**, 2172-2179 (2002).
33. D'Alessandro, M. *et al.* A tunable artificial circadian clock in clock-defective mice. *Nature communications* **6**, 8587, doi:10.1038/ncomms9587 (2015).
34. Gu, X. *et al.* The circadian mutation PER2(S662G) is linked to cell cycle progression and tumorigenesis. *Cell death and differentiation* **19**, 397-405, doi:10.1038/cdd.2011.103 (2012).
35. Wethmar, K. The regulatory potential of upstream open reading frames in eukaryotic gene expression. *Wiley interdisciplinary reviews. RNA* **5**, 765-778, doi:10.1002/wrna.1245 (2014).
36. Jang, C., Lahens, N. F., Hogenesch, J. B. & Sehgal, A. Ribosome profiling reveals an important role for translational control in circadian gene expression. *Genome research* **25**, 1836-1847, doi:10.1101/gr.191296.115 (2015).

37. Dunlap, J. C. Genetics and molecular analysis of circadian rhythms. *Annu Rev Genet* **30**, 579-601, doi:10.1146/annurev.genet.30.1.579 (1996).
38. Martin, M. Cutadapt removes adapter sequences from high-throughput sequencing reads. *EMBnet.journal* **17**, 10-12 (2011).
39. Langmead, B. & Salzberg, S. L. Fast gapped-read alignment with Bowtie 2. *Nature methods* **9**, 357-359, doi:10.1038/nmeth.1923 (2012).
40. Trapnell, C., Pachter, L. & Salzberg, S. L. TopHat: discovering splice junctions with RNA-Seq. *Bioinformatics* **25**, 1105-1111, doi:10.1093/bioinformatics/btp120 (2009).
41. Trapnell, C. *et al.* Transcript assembly and quantification by RNA-Seq reveals unannotated transcripts and isoform switching during cell differentiation. *Nature biotechnology* **28**, 511-515, doi:10.1038/nbt.1621 (2010).
42. Robinson, M. D. & Oshlack, A. A scaling normalization method for differential expression analysis of RNA-seq data. *Genome biology* **11**, R25, doi:10.1186/gb-2010-11-3-r25 (2010).

## Acknowledgments

We thank Lausanne Genomic Technologies Facility and Vital-IT staff for high-throughput sequencing and computational support. DG acknowledges support by: Swiss National Science Foundation (grants 128399, 157528); National Center for Competence in Research (NCCR) RNA & Disease; Fondation Pierre Mercier; Fondation Leenaards; Olga Mayenfisch Stiftung; SystemsX.ch StoNets consortium; University of Lausanne. PJ was supported by Human Frontiers Science Program long-term fellowship LT000158/2013-L.

## Author contributions

V.C.-S. and P.J. performed the experiments. V.C.-S. and A.B.A. analysed the data. D.G. and V.C.-S. wrote the paper. D.G. designed the project.

## Competing financial interests

The authors declare no competing financial interests.